Ka-Band Atmospheric-Induced Temperature Fluctuations

D. D. Morabito[1]

A series of experiments was conducted for the purpose of characterizing the effects of short-term atmospheric-induced temperature fluctuations at 32 GHz (Ka-band) at DSS 13 in Goldstone, California. Total power radiometer (TPR) data were acquired at both 8.4-GHz (X-band) and Ka-band frequencies at 1-s integrations rather than the usual 5-s integrations. This effort to characterize the magnitude and statistics of atmospheric-induced system temperature fluctuations at short time scales (about 1 s) is motivated by the need to predict their effect on Ka-band spacecraft telemetry during cloudy or rainy weather conditions.

The TPR zenith sky temperature fluctuations presented in this article at 1-s time scales were found to be dominated by system noise and gain instability during clear weather conditions and by the wet troposphere during turbulent cloudy/rainy weather.

I. Introduction

Several DSN telecommunications studies have shown that, by utilizing 32.0 GHz (Ka-band) instead of 8.4 GHz (X-band) as a spacecraft-to-ground communications frequency, an advantage of approximately 7 dB (factor of 5 improvement) can be realized [1,2]. This link advantage can be used to increase data volume, decrease transmission time, decrease transmitter power on the spacecraft, decrease spacecraft antenna size, or allow for a smaller antenna on the ground. The advantage is due to increased antenna gain at the shorter wavelengths. However, in practice, the advantage is reduced by higher atmospheric noise, antenna performance deficiencies, and weather susceptibility at Ka-band. The use of Ka-band as a telecommunications link frequency has been demonstrated using spacecraft signals. This was accomplished using Mars Observer [3], Mars Global Surveyor [4], and Deep Space 1 [5], which all transmitted simultaneously at both X-band and Ka-band. The use of Ka-band was also studied by analyzing the received carrier signals for Mars Observer [3], Mars Global Surveyor [4,6], Deep Space 1 [6], and Cassini [6,7].

The signal degradation due to weather, principally rain, has been a major concern for Earth-orbiting satellite systems, which operate at Ka-band. A number of programs, such as the Advanced Communications Technology Satellite (ACTS), have attempted to quantify the rain-fade problem at Ka-band. ACTS

[1] Communications Systems and Research Section.

The research described in this publication was carried out by the Jet Propulsion Laboratory, California Institute of Technology, under a contract with the National Aeronautics and Space Administration.

was an experimental satellite developed and operated by NASA and its contractors in the United States [8]. It was launched in September 1993, and the experiments were completed in May 2000 [8]. Ka-band propagation experiments using ACTS included statistical measurements on fade depths and fade times as a function of rain rate at 20.2 GHz and 27.5 GHz [9]. The impact of rain-fade compensation protocols on bit-error rate (BER) performance using ACTS with very small-aperture terminal (VSAT) ground stations was addressed by Cox and Coney [10]. Techniques were presented for ground stations to first detect the presence of a fade and then adaptively compensate for it by invoking mitigation measures such as burst-rate reduction and forward-error correction. However, for deep-space communications, where the round-trip light times can range from a sizable fraction of an hour to several hours, such techniques are not feasible. The use of improved weather forecasting to allow for an optimum link scenario (data rate and modulation index for a given percent weather) to be set up prior to a tracking pass is being developed as a tool to optimize data return.[2] Strategies have been studied for maximizing data return using Ka-band over a wide range of possible weather conditions [11].

A previous experiment involved analyzing system operating noise temperature, T_{op}, data acquired during the Summer Undergraduate Research Fellowship Satellite 1 (SURFSAT-1) link experiment at the 34-m research and development (R&D) antenna, DSS 13, at Goldstone, California, to estimate the noise contribution due to the atmosphere at both Ka-band and X-band [12]. Data from 192 tracking passes conducted between November 1995 and October 1996 were acquired over a wide range of elevation angles (or air masses). The T_{op} data were recorded at about 5-s intervals as the antenna tracked the spacecraft in elevation angle (antenna "tipping" curves). The statistics and cumulative distributions of these measurements were presented, along with intercomparisons of independent estimates derived from concurrent water vapor radiometer (WVR) data and a model using input surface meteorological data. General agreement was found between the total power radiometer (TPR) data and the WVR data, but the model using surface meteorological data was found to be deficient during cloudy and rainy weather conditions for the obvious reason that the data were sampled by ground sensors and did not account for contributions higher up.

The focus of this article is to characterize short-time-scale (∼1-s) atmospheric-induced effects and predict their impact on Ka-band spacecraft telemetry links during turbulent weather conditions, and to infer the magnitude of such fluctuations. This article reports on the results of a series of experiments conducted at Goldstone, California, for the purpose of evaluating atmospheric temperature fluctuation effects at Ka-band. The 34-m beam-waveguide (BWG) antenna, DSS 13, was used, acquiring TPR data at both X-band and Ka-band. The TPR provided 1-s integrations rather than the usual 5-s integrations in order to allow characterization of atmospheric-induced fluctuations on shorter time scales

II. Statistical Models and Theory

The TPR provides estimates of noise temperature, T_{op}, for two independent frequency bands. The input X-band and Ka-band intermediate frequency (IF) channels are filtered using one of several available filters with bandwidth B. The integration time, T, was set to 1 s for these experiments. The relative system noise floor (or thermal noise) for the TPR measurements is given by the following:

$$\frac{\sigma_{Top}}{T_{op}} = \frac{1}{\sqrt{B\mathrm{T}}} \tag{1}$$

Given a set of T_{op} measurements, the mean and standard deviation of the measurements can be estimated and compared with the predicted thermal noise contribution in Eq. (1), or with that of other

[2] S. Slobin, personal communication, Jet Propulsion Laboratory, Pasadena, California, July 18, 2002.

noise contributions. In order to assess the noise contributions at various time scales, the Allan standard deviation (ASD) of the relative temperature measurements is estimated using the definitions in [13].

The fractional temperature averaged over an interval τ at sample time t_k is given by

$$z_k = \left(\frac{T_{op}(t_k + \tau) - T_{op}(t_k)}{\overline{T}_{op}} \right)_k$$

where $\overline{T}_{op}$ is the average system temperature, which is used to normalize the relative temperature measurements. A series of measurements is acquired with $t_{k+1} = t_k + \tau,\ k = 1, 2, 3, \cdots, N$, with each measurement averaged over a time interval τ. For a set of N samples, each taken over this time interval and repetition period, the ASD is then given by [13]:

$$\sigma_z(\tau) = \sqrt{\left\langle (z_k - \bar{z}_k)^2 \right\rangle} \tag{2}$$

Thus, the fluctuations of the relative temperature measurements given in Eq. (2) can be analyzed as a function of time scale. The atmospheric-dominated fluctuations are expected to affect the received signal signal-to-noise ratio (SNR) through attenuation and thermal noise. To infer the effect of these temperature fluctuations on signal phase (or frequency), we can project the relative temperature fluctuations to relative frequency fluctuations. The resulting ASD of the relative frequency fluctuations can then be compared with the ASD measured from the carrier signal frequency residuals. These inferred effects on signal phase are the focus of further study.

III. Experiment Configuration

The ground station used to acquire the data is DSS 13, a 34-m BWG antenna located at the NASA Goldstone Deep Space Communications Complex near Barstow, California. DSS 13 is an R&D antenna, which was the prototype for the DSN BWG subnet. This antenna incorporates a series of mirrors inside beam-waveguide tubes, which direct the energy into a subterranean pedestal room, and also provides a relatively stable environment for the feed and electronics equipment. Such an arrangement provides easy access to multiple feeds located at different positions on a circular ring as compared to antennas, which have a single package in a feed cone mounted on the main-reflector surface. In addition, since the feed packages are located inside the subterranean room, there is less susceptibility to weather effects.

A "weather system" samples and records a range of meteorological parameters, including atmospheric pressure, air temperature, relative humidity, wind speed, and wind direction. These measurements can be used to predict atmospheric noise temperature and attenuation based on a surface model. These predictions based on weather data are of reasonable accuracy during clear, dry conditions, but become increasingly inaccurate during wetter, more turbulent conditions.

A detailed discussion of the DSS-13 subsystems that were used to acquire the data is provided in [14].

A summary of the experiments conducted at DSS 13 in order to characterize 1-s temperature fluctuations at Ka-band (and X-band) is provided in Table 1.

Calibrations called minicals were performed at the start of each experiment to calibrate the system gain, measure system linearity, and characterize system-induced noise statistics. During each calibration, the TPR measures the receiver output power at an IF while the low-noise amplifier input is switched from (1) sky, to (2) sky plus noise diode, to (3) ambient load, to (4) ambient load plus noise diode. The

measurements are converted into a transfer function (T_{op} versus total noise power) and also allow for the correction of any nonlinearity, which may be present. For the methodology and techniques used for system calibration, see Stelzried and Klein [15]. Table 2 presents a summary of the minicals for the experiments. The gain stability (or gain figure of merit $\Delta G/G$) is a measure of the relative scatter of the system gain to the mean gain measured over the set of minical measurements, which are usually of 2 minute duration. Typically, about 5 minicals are performed in succession prior to the start of a track. The system nonlinearity parameter describes the deviation of system gain versus temperature. The average values of the X-band and Ka-band system temperatures measured during the minical measurements are also given in Table 2.

IV. TPR Experiment Results

The series of experiments performed during the latter half of 2001 at DSS 13 for the purpose of characterizing system temperature fluctuations on short, ∼1-s time scales at Ka-band will be addressed in this section. The TPR data were acquired at 1-s averages and 1-s spacing between measurements. The TPR measurements were acquired for sufficiently long arcs of time (∼1 hour) while on ambient loads for passes 2001/243 and 2001/348, and while pointed at zenith sky for passes 2001/243, 2001/329-330, 2001/332-333, and 2001/348 (see Table 1). Pass 2001/282 was used primarily to characterize system performance using different TPR filter bandwidths.

Table 1. TPR experiment summary.

Experiment	2001 date	Zenith sky data, start–stop UTC	Weather Conditions
2001/243	August 31	17:00–22:40	Fair
2001/282	October 9	—	Fair
2001/329-330	November 25–26	06:00–15:30	Fair
2001/332-333	November 28–29	21:30–09:00	Rainy/cloudy/cold
2001/348	December 14	19:40–20:48	Cloudy, then clear

Table 2. Calibration summary.

Experiment	Band	$\Delta G/G$	System linearity factor	$T_{\rm zenith}$, K	$T_{\rm load}$, K
2001/243	X	0.00087	0.9918	44.23 ± 0.04	314.96 ± 0.02
2001/282	X	0.00064	1.0013	44.40 ± 0.04	314.87 ± 0.12
2001/329-330	X	—	0.9981	44.35 ± 0.008	311.00 ± 0.30
2001/332-333	X	0.01007	1.0014	44.57 ± 0.15	311.37 ± 0.44
2001/348	X	0.00168	0.9967	45.36 ± 0.35	311.87 ± 0.02
2001/243	Ka	0.00127	1.0033	74.03 ± 0.09	346.97 ± 0.04
2001/282	Ka	0.00181	1.0044	73.62 ± 0.14	346.96 ± 0.11
2001/329-330	Ka	0.00139	—	71.43 ± 0.26	343.11 ± 0.26
2001/332-333	Ka	0.02721	—	74.69 ± 1.84	343.35 ± 0.46
2001/348	Ka	0.00106	—	90.63 ± 3.49	343.79 ± 0.02

The average values and scatter of the ambient and zenith temperature measurements over their respective acquisition periods were computed as one set of statistical measurements. In addition, the ASD of the relative temperature fluctuations, $\sigma_z(\tau)$, was computed to characterize the fluctuation energy over time intervals of $\tau = 1, 10, 100$ and 1000 s. The average values and scatter of the temperature measurements and the ASDs of the relative temperature measurements are presented for X-band while on ambient load in Table 3, for Ka-band while on ambient load in Table 4, for X-band while the antenna is pointed at zenith in Table 5, and for Ka-band while the antenna is pointed at zenith in Table 6. The values can be compared with other system or atmospheric noise contributions predicted by other means, such as gain instability as measured during the minicals, thermal noise using equation Eq. (1) based on the TPR filter bandwidth and integration time, and measured fluctuations from weather or WVR sky-brightness temperature data at appropriate time scales.

Table 3. X-band ambient system temperature statistical summary.

Experiment	Average, K	$\sigma_z(\tau = 1$ s)	$\sigma_z(\tau = 10$ s)	$\sigma_z(\tau = 100$ s)	$\sigma_z(\tau = 1000$ s)
2001/243	315.185 ± 0.308	0.000288	0.000231	0.000316	—
2001/348	312.787 ± 0.254	0.000377	0.000241	0.000335	0.000554

Table 4. Ka-band ambient system temperature statistical summary.

Experiment	Average, K	$\sigma_z(\tau = 1$ s)	$\sigma_z(\tau = 10$ s)	$\sigma_z(\tau = 100$ s)	$\sigma_z(\tau = 1000$ s)
2001/243	349.075 ± 0.874	0.000519	0.000529	0.000770	—
2001/348	341.902 ± 0.348	0.000447	0.000280	0.000334	0.000268

Table 5. X-band zenith system temperature statistical summary.

Experiment	Average, K	$\sigma_z(\tau = 1$ s)	$\sigma_z(\tau = 10$ s)	$\sigma_z(\tau = 100$ s)	$\sigma_z(\tau = 1000$ s)
2001/243	44.181 ± 0.076	0.000397	0.000243	0.000360	0.000818
2001/329-330	44.230 ± 0.167	0.000314	0.000248	0.000305	0.000719
2001/332-333	44.904 ± 0.417	0.000431	0.00113	0.00214	0.00378
2001/348	44.949 ± 0.520	0.000595	0.00180	0.00338	0.00886

Table 6. Ka-band zenith system temperature statistical summary.

Experiment	Average, K	$\sigma_z(\tau = 1$ s)	$\sigma_z(\tau = 10$ s)	$\sigma_z(\tau = 100$ s)	$\sigma_z(\tau = 1000$ s)
2001/243	74.949 ± 0.234	0.000599	0.000539	0.000673	0.00130
2001/329-330	72.972 ± 0.553	0.000490	0.000516	0.000739	0.00140
2001/332-333	74.595 ± 2.917	0.00174	0.00641	0.0122	0.0192
2001/348	84.582 ± 9.781	0.00269	0.0109	0.0181	0.0940

A. Details on Individual Experiments

1. Pass 2001/243 (August 31, 2001). The experiment conducted on 2001/243 (August 31, 2001) consisted of (1) performing a series of minicals at both frequency bands in order to characterize system linearity and system gain stability, (2) acquiring 1 hour of data while on the ambient loads in order to characterize the system performance and fluctuations on the system up to the ambient-load, and (3) acquiring about 6 hours of data while the antenna was pointed at zenith in order to characterize fluctuation information at short time scales. The weather was relatively clear that day.

The minicals, summarized in Table 2, were performed during the first hour of the pass and showed good system linearity and gain stability.

System temperature data were acquired while on the ambient load between 16.2 and 17.1 hours UTC.

The zenith cold-sky system-temperature measurement time series were then acquired continuously over 18,214 s. The weather conditions were nominal, as exhibited by the nominal 74.9-K zenith system noise temperature at Ka-band.

2. Pass 2001/282 (October 9, 2001). This pass was conducted at both X-band and Ka-band for the purpose of evaluating the effect of using several different filter bandwidths on the TPR. Filter bandwidths of 4.68, 10, 20, 30, 92, and 500 MHz were used on both bands. The fluctuations of the TPR measurements indicate that gain instability dominates at both frequency bands. The minical measurements are summarized in Table 2. No significant difference between filters was generally detectable, as the fluctuations of the measurements were consistent between segments using the different filters. The fluctuations appeared to be limited by gain instability for almost all cases. For those few cases where the measurement noise exceeded the scatter expected due to gain instability, the antenna was pointed on cold sky and the measurements were elevated above the estimated values inferred from minical measurements for both X-band and Ka-band, suggesting a sizable atmospheric contribution.

3. Pass 2001/329-330 (November 25–26, 2001). It was anticipated that this experiment would be conducted during turbulent conditions. However, by the time the experiment was initiated, the weather conditions were fair. About 19,726 seconds of continuous TPR data were acquired while the antenna was pointed at zenith.

4. Pass 2001/332-333 (November 28–29, 2001). A long time arc of zenith cold-sky measurements was acquired for the cloudy/rainy weather pass conducted on 2001/332-333 (November 28–29, 2001). Significant fluctuations due to weather were observed for this pass, which is classified as a rainy/cloudy weather pass.

5. Pass 2001/348 (December 14, 2001). The sky started out cloudy and wet and then cleared up during the course of this pass. The station chose to acquire the zenith sky temperature measurements first in order to capture fluctuations due to turbulent weather, as it was obvious that the sky was clearing. After acquiring an hour of zenith sky data, the station acquired about an hour of data while on the ambient load.

B. Discussion on Ambient-Load TPR Data

The two passes in which sufficiently long time periods of ambient-load TPR data were acquired were 2001/243 (clear weather) and 2001/348 (cloudy/rainy weather). The ambient-load system temperature time series for pass 2001/243 are shown in Figs. 1 and 2 for X-band and Ka-band, respectively. The statistics are shown in Table 3 for X-band and Table 4 for Ka-band. The ASDs of the 2001/243 relative temperature fluctuation time series are displayed in Figs. 3 and 4 for X-band and Ka-band, respectively. The ambient-load system-temperature measurements and corresponding Allan deviation measurements for pass 2001/348 are consistent with those of pass 2001/243, for both frequency bands.

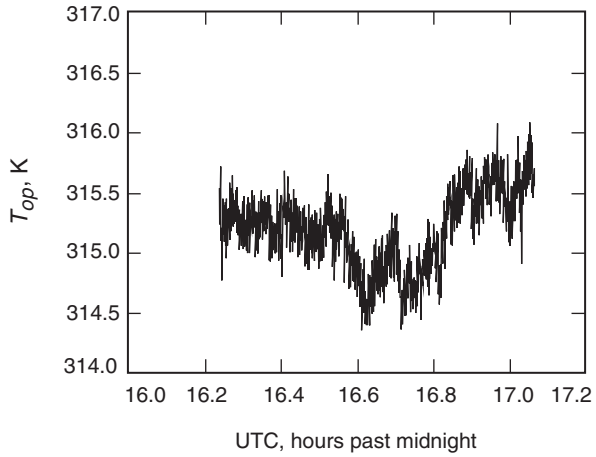

Fig. 1. 2001/243 X-band ambient-load T_{op}.

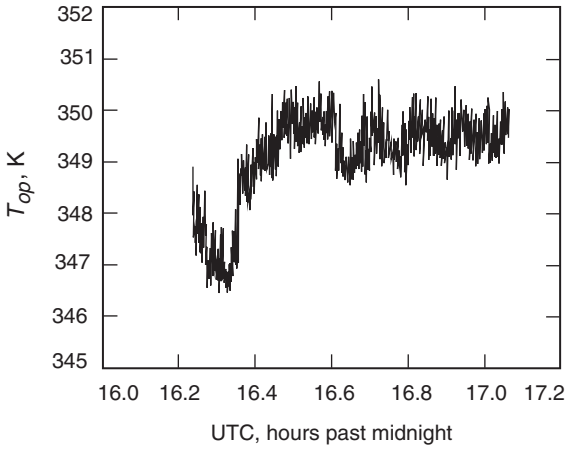

Fig. 2. 2001/243 Ka-band ambient-load T_{op}.

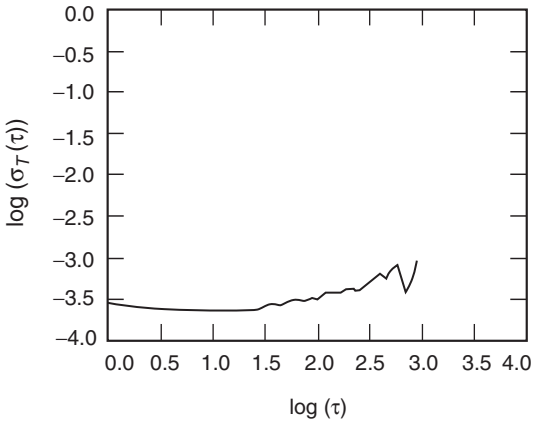

Fig. 3. 2001/243 X-band ambient-load T_{op} Allan deviation.

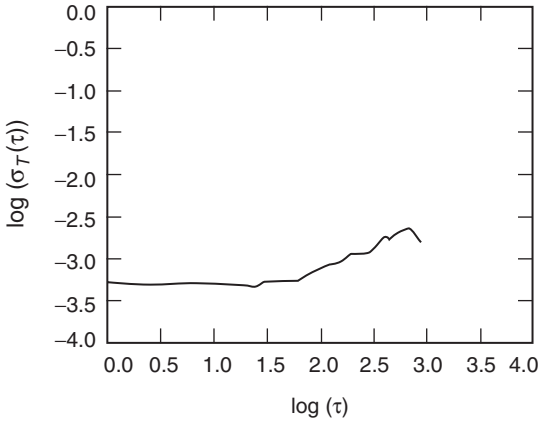

Fig. 4. 2001/243 Ka-band ambient-load T_{op} Allan deviation.

The ASD values for the floors between 1 s and ∼100 s for both frequency bands are roughly consistent with values of the gain instability measured by the minicals conducted at the start of each experiment. Since a series of minicals is performed over durations of several minutes, the scatter of the gain about the mean gain provides an estimate of the gain instability over this time scale, which can then be compared with the measured fluctuations in the TPR data. Since the minicals and ambient-load data were acquired at disjointed time periods, they are not expected to agree exactly, as they temporally vary depending upon environmental conditions. These ambient-load short-time-scale fluctuations characterize the system excluding the atmosphere. The thermal noise contributions for pass 2001/243 using the 92-MHz filter bandwidths are estimated to be about 0.01 percent (0.0001), which lies below the estimated gain stability values and the ASD floors for both X-band and Ka-band 2001/243 data.

C. Discussion on Zenith Sky TPR Data

The TPR measurements acquired while the antenna was pointed at zenith for the four passes in Tables 5 and 6 for X-band and Ka-band, respectively, will be discussed here. The zenith cold-sky measurement time series for pass 2001/243 are shown in Figs. 5 and 6 for X-band and Ka-band, respectively. The corresponding Allan deviation plots are displayed in Figs. 7 and 8 for X-band and Ka-band, respectively.

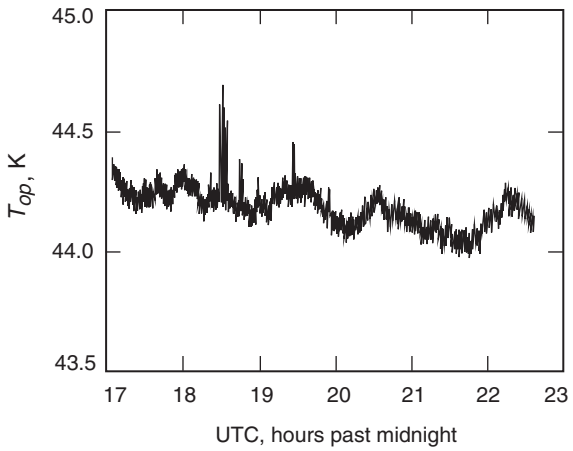

Fig. 5. 2001/243 X-band zenith-sky T_{op}.

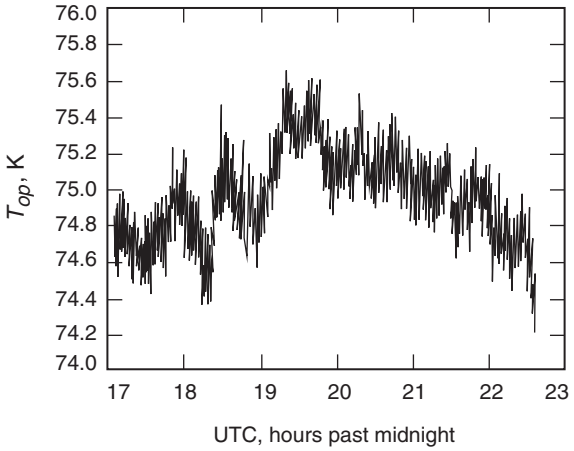

Fig. 6. 2001/243 Ka-band zenith-sky T_{op}.

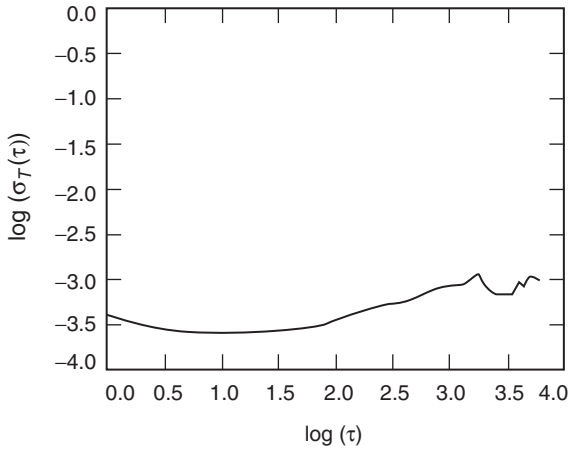

Fig. 7. 2001/243 X-band zenith-sky T_{op} Allan deviation.

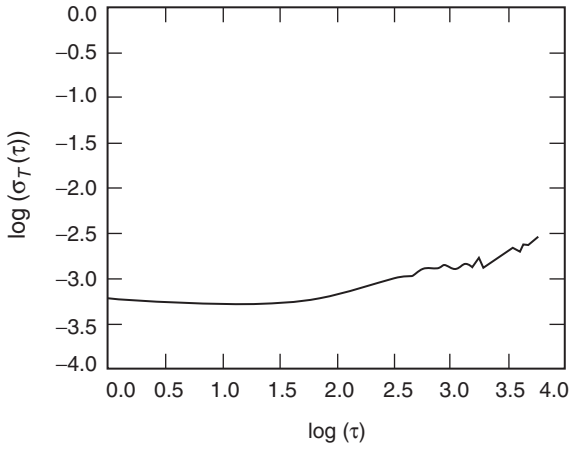

Fig. 8. 2001/243 Ka-band zenith-sky T_{op} Allan deviation.

The values and signatures of the temperature ASDs for the zenith cold sky show no significant increase over those of the ambient load in Figs. 3 and 4 between 1-s and 1000-s time scales, suggesting that system effects, and not atmosphere, dominate during the clear weather conditions, which were present for this experiment.

The zenith cold-sky measurement time series for pass 2001/329-330 as well as their corresponding ASD plots are very similar to those of pass 2001/243 provided in Figs. 5 through 8. The values and signatures of the ASDs for the zenith cold sky show no significant increase over those of the 2001/243 ambient-load ASDs (Figs. 3 and 4) and the 2001/243 zenith sky temperature ASDs (Figs. 7 and 8) between 1 s and 1000 s, suggesting again that system effects, and not atmosphere, are the dominating contributors observed during these clear weather conditions.

There are long period trends in the X-band and Ka-band TPR data for pass 2001/329-330 (not shown here), which contribute to the increase in the ASD at long time intervals above 1000 s. These long period trends are attributed to uncalibrated gain variations, which are of different signs for the X-band and Ka-band equipment packages, as the pedestal room is not temperature stabilized (minicals cannot be performed at the same time in which continuous TPR data are acquired). A minical conducted at the end of

the experiment showed a significant gain calibration correction at Ka-band with a zenith sky temperature of 71 K, which is in agreement with the values measured near the start of the pass.

The zenith cold-sky measurement time series for the cloudy/rainy weather pass conducted on 2001/332-333 (November 28–29, 2001) are shown in Figs. 9 and 10 for X-band and Ka-band, respectively. There are significant fluctuations at both bands, which are correlated. The corresponding relative-temperature ASDs are displayed in Figs. 11 and 12 for X-band and Ka-band, respectively. The signatures of these ASD measurements appear to be significantly different (more positively sloped) than those of the previous experiment clear-weather zenith-sky temperature ASDs and ambient-load ASDs. Near the 1-s time scale, $\log(\tau) = 0$, the log(ASD) value of -3.3 for the X-band zenith sky shows no significant increase over that of the clear-weather passes 2001/243 (-3.4 in Fig. 7) and 2001/329-330 (-3.5). However, there are significantly increased levels of ASD for time scales of 10 s and above. For Ka-band zenith sky, near the 1-s time scale ($\log(\tau) = 0$), the value of log(ASD) $= -2.8$ (in Fig. 12) is significantly higher than those for the clear-weather passes 2001/243 (-3.2 in Fig. 8) and 2001/329-330 (-3.3). In addition, significantly increased values of ASD are apparent for time scales above 10 s. Based on very low air temperature ($\sim$4 deg C) and relative humidity measurements from the surface weather data, the temperature contributions due to water vapor are expected to be small. Since cold air holds very little water vapor

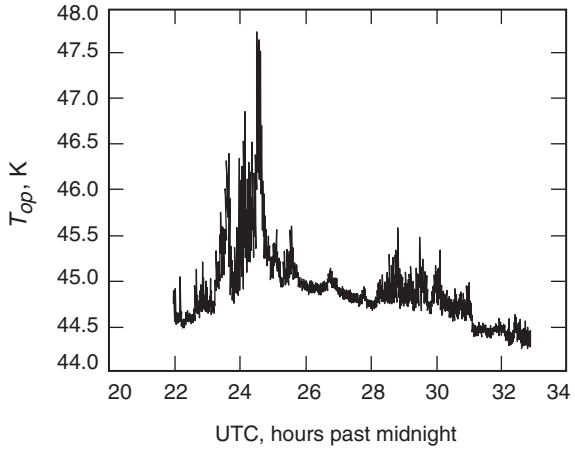

Fig. 9. 2001/332-333 X-band zenith-sky T_{op}.

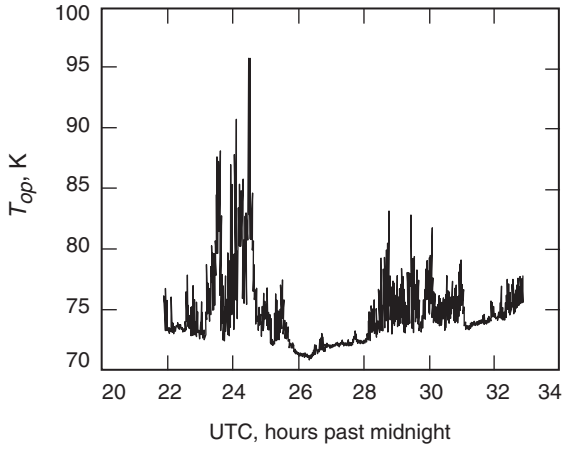

Fig. 10. 2001/332-333 Ka-band zenith-sky T_{op}.

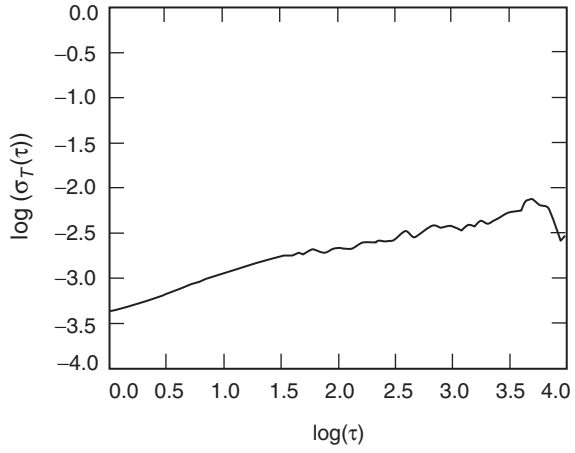

Fig. 11. 2001/332-333 X-band zenith-sky T_{op} Allan deviation.

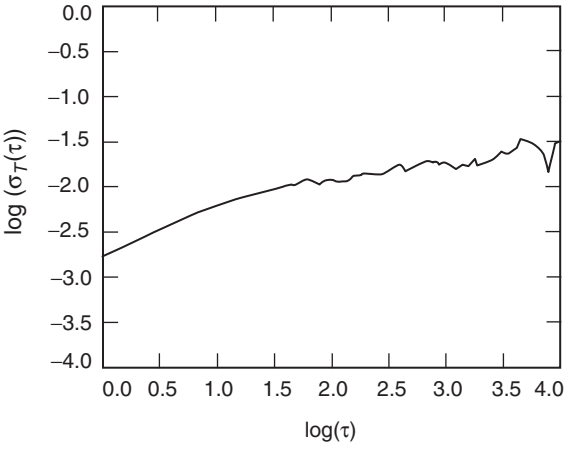

Fig. 12. 2001/332-333 Ka-band zenith-sky T_{op} Allan deviation.

at these temperatures, the significant variations seen in these data are attributed to cloud precipitants (liquid water) higher up in the atmosphere (away from the surface weather sensors) as they cross the antenna beam pointed at zenith. The contributions due to liquid water would be expected to have a lesser effect on path delay rate (frequency), and their principal effect would be on the system temperature, which would affect the received signal SNR of any spacecraft being tracking. The atmospheric fluctuations on received SNR appear to be the dominating atmospheric factor affecting telemetry reception, as opposed to atmospheric-induced phase fluctuations. However, these effects may decrease as the time scales become shorter (below 1 s) due to beam averaging [16] and merit further study.

Pass 2001/348 started out cloudy and wet and then cleared up, as exhibited by the zenith system noise temperature measurements of Figs. 13 and 14 for X-band and Ka-band, respectively. Note that there is a significantly elevated level of system temperature (47 K for X-band and about 110 K for Ka-band) above the clear-weather nominal values (44 K for X-band and 73 K for Ka-band) with significant temperature fluctuations occurring at both bands at the start of the pass. The level of the background system noise temperature reduces to nominal "clear" weather system temperature levels by the end of the pass (44.5 K for X-band and about 73 K for Ka-band). The corresponding relative-temperature ASDs are displayed in Figs. 15 and 16 for X-band and Ka-band, respectively. The signatures of these ASD measurements

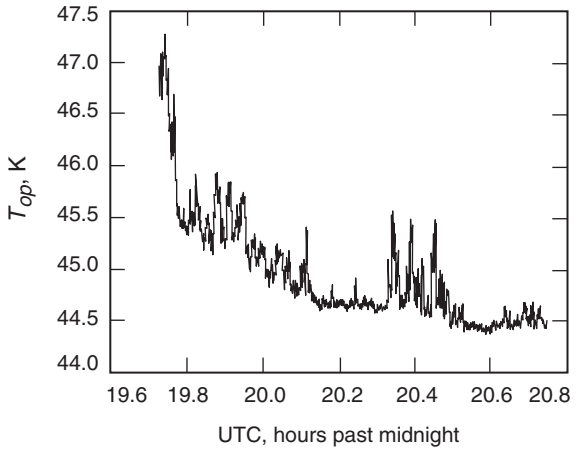

Fig. 13. 2001/348 X-band zenith-sky T_{op}.

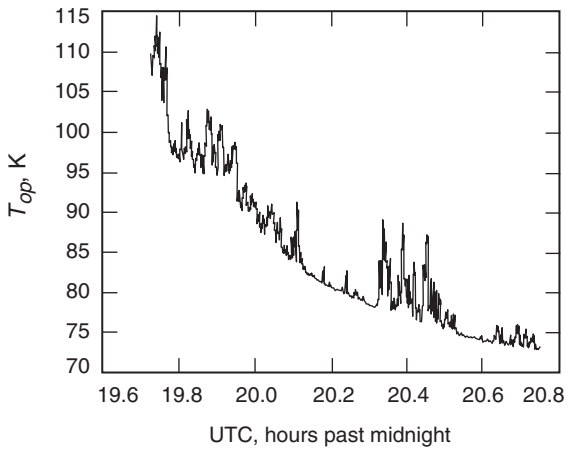

Fig. 14. 2001/348 Ka-band zenith-sky T_{op}.

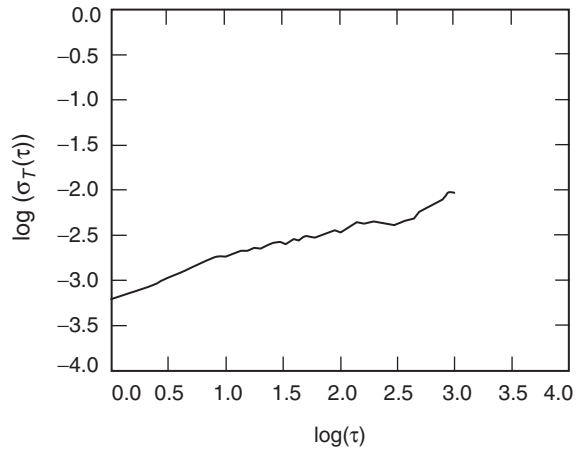

Fig. 15. 2001/348 X-band zenith-sky T_{op} Allan deviation.

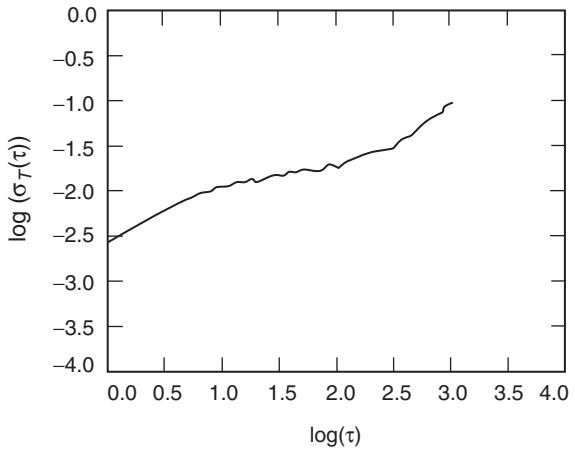

Fig. 16. 2001/348 Ka-band zenith-sky T_{op} Allan deviation.

are significantly elevated over those of the previous clear-weather passes and are more sloped than those of the other cloudy weather pass, 2001/332-333 (Figs. 11 and 12). Since both X-band and Ka-band zenith system temperatures show the same decreasing signatures and change in expected proportions due to atmosphere, the long-term variations are attributed to atmosphere rather than the system (the station visually confirmed that the sky was clearing up during this period). Near the 1-s time scale, the ASD for Ka-band at zenith is again significantly increased over those of the previous ambient-load and clear-weather zenith temperature measurements. The ASD values are significantly elevated at time scales above 10 s. The Ka-band ASD for 1-s to 10,000-s time intervals appears to be weather dominated. The TPR for experiment 2001/348 utilized 20-MHz filters for both bands, resulting in an expected TPR thermal noise floor of $\Delta T/T = 0.000224$ ($\log(\text{ASD}) = -3.65$) at 1 s.

V. Example of Turbulent Weather during a Spacecraft Pass

The Mars Global Surveyor (MGS) spacecraft, launched on November 7, 1996, carried an experimental space-to-ground telecommunications link at Ka-band (32 GHz) in addition to the primary X-band (8.4-GHz) downlink [4]. A Ka-band link experiment using MGS, known as the Ka-Band Link Experiment II (KaBLE-II), allowed the performances of the Ka-band and X-band signals to be compared under nearly identical conditions, as they were regularly tracked during the 2-year period between 1997 and 1998. This experiment included acquisition of carrier-signal-level data, P_c/N_o, and TPR data for both X-band and Ka-band acquired over a wide range of station elevation angles, weather conditions, and solar elongation angles. The measurements confirmed the expected Ka-band link advantage over X-band. The MGS/KaBLE-II link experiment measured signal strengths (for 54 percent of the experiments conducted), which were in reasonable agreement with predicted values based on preflight knowledge, and frequency residuals, which agreed between bands and whose statistics were consistent with expected noise sources. For passes in which measured signal strengths disagreed with predicted values, the problems were traced to known deficiencies in equipment operating under certain conditions [4]. A total of 197 tracking passes for MGS/KaBLE-II were conducted between December 1996 and December 1998, with the vast majority conducted under nominal weather conditions. The TPR data acquired for the passes were sampled and integrated at 5-s intervals.

Given that the focus of the current study is to characterize the short-time-scale atmospheric effects on a received spacecraft signal at Ka-band, an especially turbulent weather pass, 1997/203, from the MGS/KaBLE-II experiment was selected for study. As the vast majority of the passes were conducted under nominal weather conditions, it is emphasized that the conditions during much of the selected experiment exceeded 99 percent weather. Thus, the likelihood is that such conditions will occur at Goldstone less than 1 percent of the time.

The TPR data acquired at DSS 13 during 1997/203 were sampled and integrated at 5-s intervals, and this pass was conducted during a very turbulent rain storm, as is apparent in Figs. 17 and 18 for X-band and Ka-band TPR data, respectively [4]. During spacecraft rise, the DSS-13 antenna was pointed into a very heavy, dark rain cell near the horizon, where thunder and lightning were prevalent, as reported by station personnel. Here, the Ka-band total system noise temperature exceeded 300 K. The corresponding Allan deviation plots are shown in Fig. 19 and 20 for X-band and Ka-band, respectively. The changes in system noise temperature due to changing elevation angle were not normalized to refer the atmosphere to one airmass at zenith, since the turbulent temporal fluctuations dominate. The ASD signatures are consistent with those expected for turbulent weather. Note that the ASDs at 10-s to 5-s time scales approach a value of about 0.001, consistent with the contribution due to gain instability at both bands. The extrapolations of the ASD signatures down to 1-s ($\log(\tau) = 0$) appear to be consistent with gain instability, at least at X-band. The minicals for this pass measured gain stability figure of merits of 0.055 percent for X-band and 0.056 percent for Ka-band. The thermal noise contribution for this experiment, using 20-MHz bandwidth filters and 5-s radiometer integration times, is estimated to be 0.01 percent (0.0001).

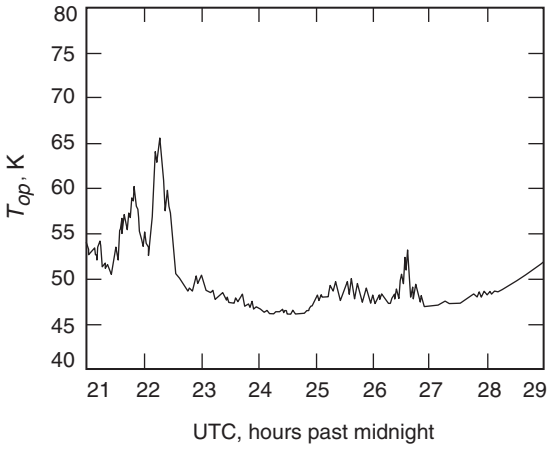

Fig. 17. MGS 1997/203 X-band T_{op}.

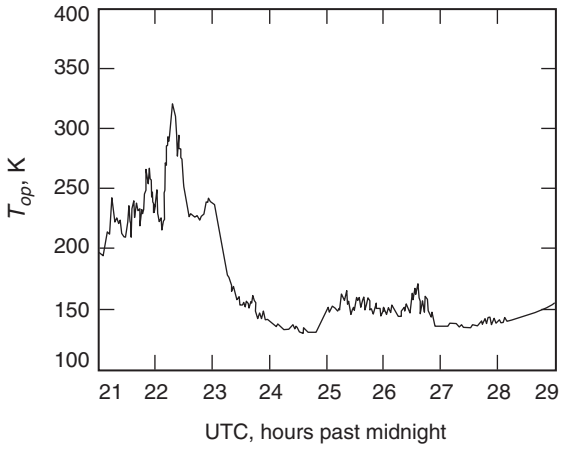

Fig. 18. MGS 1997/203 Ka-band T_{op}.

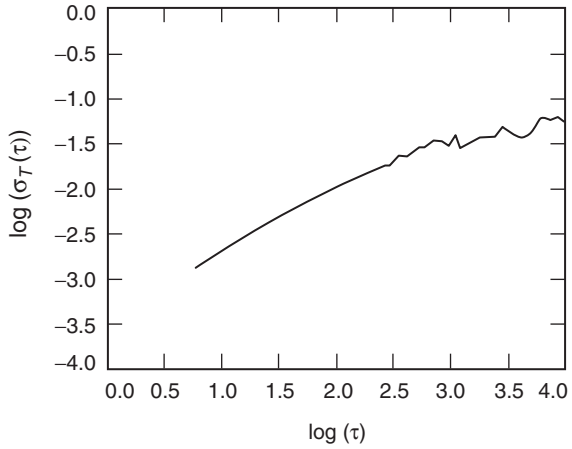

Fig. 19. MGS 1997/203 X-band T_{op} Allan deviation.

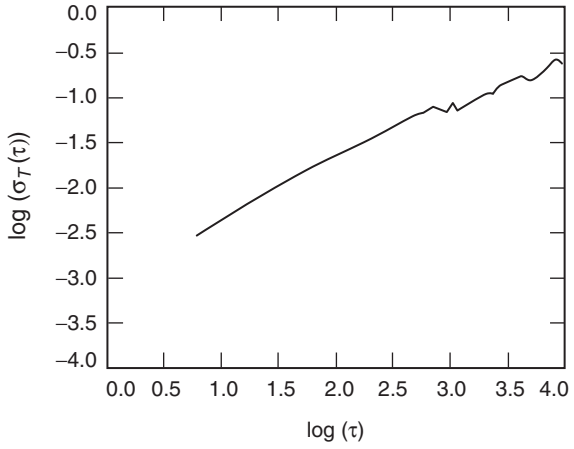

Fig. 20. MGS 1997/203 Ka-band T_{op} Allan deviation.

This pass, 1997/203, is characterized by weather that exceeds 99 percent cumulative distribution. According to the DSN 810-5 document [17], this corresponds to a zenith atmospheric contribution of 36 K to the Ka-band system temperature at zenith at Goldstone. The atmospheric contribution to the noise temperature exceeded 36 K (referenced at zenith) for much of the pass, as exhibited in the concurrent WVR sky-brightness temperature data[3] at 31.4 GHz displayed in Fig. 21. The WVR data in Fig. 21 show the same general weather behavior as the X-band and Ka-band TPR data in Figs. 17 and 18, respectively. A large storm system is apparent from the start of the pass, which dissipates by 203/23:30 UTC. A smaller scale period of increased activity and temperature is apparent between 204/01:00 and 204/03:00 UTC. The features seen in the WVR data (Fig. 21) are not expected to exactly match the features seen in the TPR data, as the WVR and DSS-13 beams are sampling different sections of sky, and the WVR data are sampled at a longer time scale.

VI. Discussion

The summary of the zenith sky temperature statistics is presented in Table 5 for X-band and Table 6 for Ka-band. The consistency of the TPR measurements is now examined. Estimated values of all

[3] S. Keihm, Jet Propulsion Laboratory, Pasadena, California, provided WVR data.

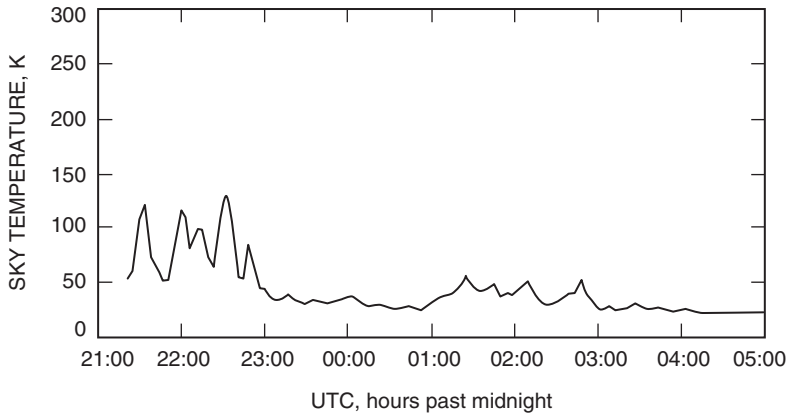

Fig. 21. Water vapor radiometer 31.4-GHz sky temperature for 1997/203.

nonatmospheric temperature contributions were subtracted from the X-band and Ka-band TPR cold-sky measurements for both 2001/243 (42.12 K at X-band and 64.93 K at Ka-band) and 2001/332-333 (42.6 K at X-band and 64.93 K at Ka-band). These values were chosen in order to make the average difference equal to weather model values (∼2.28 K at X-band and ∼8.69 K at Ka-band for 2001/243), using a weather model program.[4] Figure 22 displays the resulting X-band and Ka-band atmosphere noise temperature time signatures for pass 2001/243. Figure 23 displays the ratio of the Ka-band atmospheric noise temperature to the X-band atmospheric noise temperature, which is about four over the pass.

The atmospheric noise temperature time signatures for X-band and Ka-band are shown in Fig. 24 for pass 2001/332-333. Note that there are significant fluctuations that appear to be correlated between the two bands, but are dominating at Ka-band. The minimum Ka-band temperature is very close to the minimum value of 6 K expected, with little or no water vapor at Goldstone (consistent with the very low air temperature). The time behavior of the ratio of Ka-band to X-band atmospheric noise temperatures of Fig. 24 is shown in Fig. 25. This ratio for pass 2001/332-333 does not behave as well as that for 2001/243 (Fig. 23) and shows significant fluctuations. Although there is an expected scaling error since the weather model used surface meteorological data to calibrate out the baseline troposphere, the significant short-term fluctuation peaks are attributed to liquid water in clouds traversing the antenna beam. Ka-band is expected to be more susceptible than X-band to effects of liquid water. It should be kept in mind that the Ka-band noise temperature is also more susceptible than X-band to water vapor, although the change in path delay may be roughly the same at both frequencies.

The Ka-band to X-band atmospheric noise-temperature ratio will range from about 3.5 for dry weather (oxygen only) to about 12 (water only). Figures 23 and 25 display typical ratios of the combined dry and wet atmosphere for two different conditions. The contribution due to water significantly changes as a function of weather conditions, and this is especially evident in the changes in the ratio shown in Fig. 25, which also includes some scaling error.

The 2001/348 ambient-load and zenith-sky temperature ASD curves are displayed together on the same plot: Fig. 26 for X-band and Fig. 27 for Ka-band. The effects of the atmosphere (zenith sky) for this cloudy weather pass can then be assessed against the effects of the system (ambient load). Note that in Fig. 26 the zenith sky energy is increased above the ambient-load energy for all time scales at X-band (at 1 s the increase is small). The same general trend is apparent for Ka-band (Fig. 27) but more significant at all time scales.

[4] S. Slobin, SDS4BAS program, Jet Propulsion Laboratory, Pasadena, California.

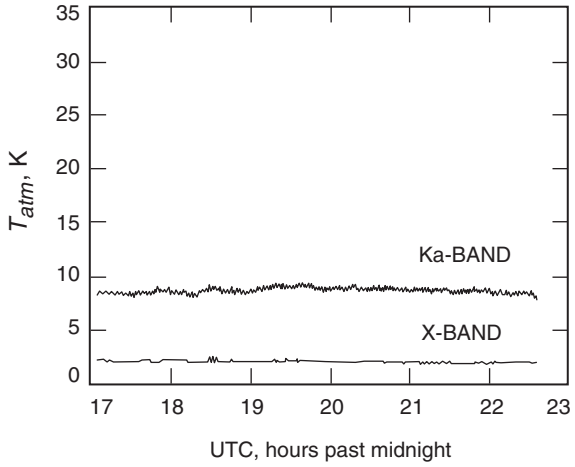

Fig. 22. 2001/243 T_{atm}.

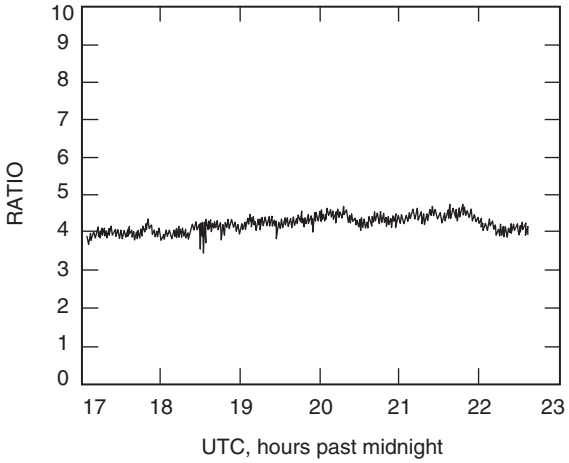

Fig. 23. 2001/243 T_{atm}(Ka)/T_{atm}(X).

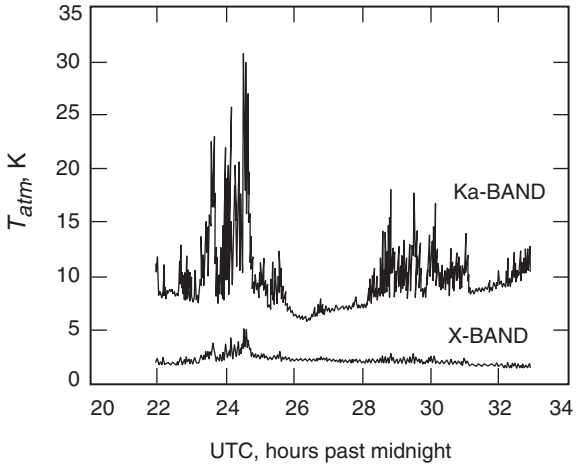

Fig. 24. 2001/332-333 T_{atm}.

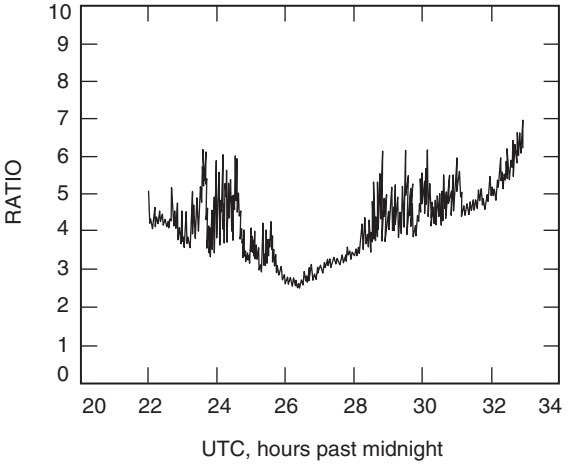

Fig. 25. 2001/332-333 T_{atm}(Ka)/T_{atm}(X).

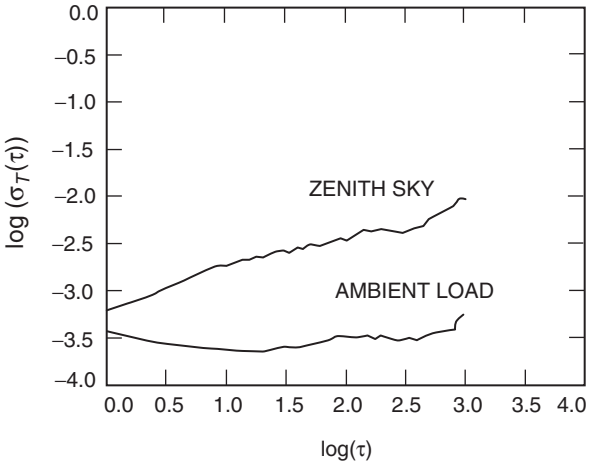

Fig. 26. 2001/348 X-band relative-temperature Allan deviation.

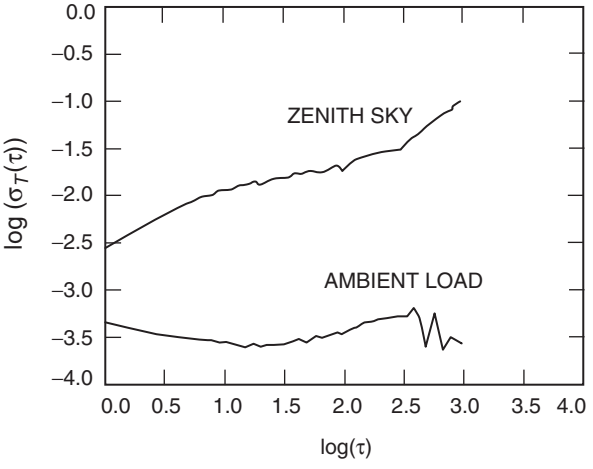

Fig. 27. 2001/348 Ka-band relative-temperature Allan deviation.

VII. Spacecraft Telemetry Considerations

The TPR zenith sky temperature data presented in this article for 1-s time scales are dominated by system noise (gain instability and thermal) during clear-weather passes and by the wet troposphere for turbulent cloudy/rainy weather passes. The effect of increased turbulent weather will be increased fluctuations on system noise temperature measurements and increased attenuation on received spacecraft signals.

All indications from the experience of Earth-orbiting satellite Ka-band operations are that, if there is sufficient margin, telemetry data can be reliably acquired, even at very high data rates. However, if a fade falls below a threshold, the data will be degraded. Thus, reliable fade depth and fade duration statistics for each tracking site need to be considered. For the DSN tracking sites of Goldstone, Madrid, and Canberra, the frequency of occurrence and average duration for fade depths of 0.5, 1, 2, and 3 dB (threshold above 90 percent cumulative temperature) were published by Pham and Townes [18]. Fading is the subject of a further study.

The tracking loop bandwidth setting of a receiver during turbulent weather passes is expected to be nominal, accounting only for the increased thermal noise resulting from the turbulence. The ASD measured from spacecraft frequency residuals appears to be sensitive only to water vapor, not liquid water, even during turbulent weather conditions.

Future work involves performing analysis or conducting experiments to assess the effects of the turbulent Ka-band troposphere on spacecraft telemetry for short time scales, which are comparable to the frame periods utilized. Such efforts would include simulations, conducting experiments using real spacecraft telemetry, theoretical analysis, and conducting additional TPR experiments at Ka-band using much shorter integration times (<1 s). The upcoming Mars Reconnaissance Orbiter (MRO) will have an active Ka-band communications link, for which several demonstrations are being planned.

Acknowledgments

I would like to thank R. Clauss, J. Armstrong, R. Hastrup, C. Naudet, L. Paal, S. Keihm, A. Tanner, and S. Shambayati for their comments, informative discussions, and suggestions; the assistance of the DSS-13 station personnel in acquiring the data; and L. Teitelbaum for scheduling the experiments. I would also like to thank J. Wyatt and R. Ceserone for their support of this work, and S. Keihm for providing WVR data used in the analysis.

References

[1] J. G. Smith, "Ka-Band (32-GHz) Downlink Capability for Deep Space Communications," *The Telecommunications and Data Acquisition Progress Report 42-88, October–December 1986*, Jet Propulsion Laboratory, Pasadena, California, pp. 96–103, February 15, 1987.
http://tmo.jpl.nasa.gov/tmo/progress_report/42-88/88M.PDF

[2] J. W. Layland and J. G. Smith, "A Growth Path for Deep Space Communications," *The Telecommunications and Data Acquisition Progress Report 42-88, October–December 1986*, Jet Propulsion Laboratory, Pasadena, California, pp. 120–125, February 15, 1987.
http://tmo.jpl.nasa.gov/tmo/progress_report/42-88/88P.PDF

[3] T. A. Rebold, A. Kwok, G. E. Wood, and S. Butman, "The Mars Observer Ka-Band Link Experiment," *The Telecommunications and Data Acquisition Progress Report 42-117, January–March 1994*, Jet Propulsion Laboratory, Pasadena, California, pp. 250–282, May 15, 1994.
http://tmo.jpl.nasa.gov/tmo/progress_report/42-117/117u.pdf

[4] D. Morabito, S. Butman, and S. Shambayati, "The Mars Global Surveyor Ka-band Link Experiment (MGS/KaBLE-II)," *The Telecommunications and Mission Operations Progress Report 42-137, January–March 1999*, Jet Propulsion Laboratory, Pasadena, California, pp. 1–41, May 15, 1999.
http://tmo.jpl.nasa.gov/tmo/progress_report/42-137/137D.pdf

[5] C. Chen, S. Shambayati, A. Makovsky, F. H. Taylor, M. Herman, S. Zingales, C. Nuckolls, and K. Siemsen, *Small Deep Space Transponder (SDST) DS1 Technology Validation Report*, JPL Publication 00-10, Jet Propulsion Laboratory, Pasadena, California, October 2000.

[6] D. D. Morabito, S. Shambayati, S. Finley, D. Fort, J. Taylor, and K. Moyd, "Ka-band and X-band Observations of the Solar Corona Acquired During Solar Conjunctions of Interplanetary Spacecraft," *Proceedings of the 7th Ka-band Utilization Conference*, Santa Margherita Ligure, Italy, Istituto Internazionale delle Communicazioni, September 26, 2001.

[7] D. D. Morabito, S. Shambayati, S. Finley, and D. Fort, "The Cassini May 2000 Solar Conjunction," accepted for publication in *IEEE Transactions on Antennas and Propagation*.

[8] S. Johnson, R. Acosta, and W. Gauntner, "Impact of Various Fade Mitigation Techniques Using Data from the ACTS Propagation Campaign," AIAA 19th International Communications Satellite Systems Conference, Toulouse, France, April 2001.

[9] R. Crane and D. Rogers, "Review of the Advanced Communications Technology Satellite (ACTS) Propagation Campaign in North America," *IEEE Antennas & Propagation Magazine*, vol. 40, no. 6, pp. 23–28, December 1998.

[10] C. Cox and T. Coney, "Advanced Communications Technology Satellite (ACTS) Fade Compensation Protocol Impact on Very Small-Aperture Terminal Bit Error Rate Performance," *IEEE Journal on Selected Areas in Communications*, vol. 17, no. 2, pp. 173–179, February 1999.

[11] S. Shambayati, "Maximization of Data Return at X-band and Ka-Band on the DSN's 34-Meter Beam-Waveguide Antennas," *The Interplanetary Network Progress Report 42-148, October–December 2001*, Jet Propulsion Laboratory, Pasadena, California, pp. 1–20, February 15, 2002.
http://ipnpr.jpl.nasa.gov/tmo/progress_report/42-148/148E.pdf

[12] D. Morabito, R. Clauss, and M. Speranza, "Ka-Band Atmospheric Noise-Temperature Measurements at Goldstone, California, Using a 34-Meter Beam-Waveguide Antenna," *The Telecommunications and Data Acquisition Progress Report 42-132, October–December 1997*, Jet Propulsion Laboratory, Pasadena, California, pp. 1–20, February 15, 1998.
http://tmo.jpl.nasa.gov/tmo/progress_report/42-132/132B.pdf

[13] R. Vessot, "Frequency and Time Standards," *Methods of Experimental Physics*, vol. 12, part C, *Astrophysics, Radio Observations*, edited by M. Meeks, New York: Academic Press, pp. 198–227, 1976.

[14] D. D. Morabito, "The Efficiency Characterization of a 34-Meter Beam-Waveguide Antenna at Ka-band (32.0 GHz) and X-band (8.4 GHz)," *IEEE Antennas & Propagation Magazine*, vol. 41, no. 4, pp. 23–34, August 1999.

[15] C. T. Stelzried and M. J. Klein, "Precision DSN Radiometer Systems: Impact on Microwave Calibrations," *Proc. of the IEEE*, vol. 82, pp. 776–787, May 1994.

[16] R. Linfield, "The Effect of Aperture Averaging Upon Tropospheric Delay Fluctuations Seen With a DSN Antenna," *The Telecommunications and Data Acquisition Progress Report 42-124, October–December 1995*, Jet Propulsion Laboratory, Pasadena, California, pp. 1–7, February 15, 1996.
http://tmo.jpl.nasa.gov/tmo/progress_report/42-124/124A.pdf

[17] *DSMS Telecommunications Link Design Handbook*, JPL 810-005, Rev. E, Jet Propulsion Laboratory, Pasadena, California, issue date January 15, 2001, JPL D-19379, Rev. E., Module 105.

[18] T. Pham, and S. Townes, "Migration Plan Toward Ka-Band Operations in the Deep Space Network," AIAA paper 2002-2068, 20th AIAA International Communication Satellite Systems Conference and Exhibit, Montreal, Quebec, May 12–15, 2002.